Journal of Applied Fluid Mechanics, Vol. 17, No. 8, pp. 1717-1729, 2024.
Available online at www.jafmonline.net, ISSN 1735-3572, EISSN 1735-3645.
https://doi.org/10.47176/jafm.17.8.2417

Numerical Simulation of Exhaled Particle Transmission in a Car Cabin with Open Windows

Y. W. Yan[1], J. J. Xu[1], J. Hu[2], Z. R. Huang[1], K. Zhong[1], and H. W. Jia[1†]

[1] *School of Environmental Science and Engineering, Donghua University, Shanghai 201620, China*
[2] *Department of Refrigeration and Air Conditioning, Shanghai Ocean University, Shanghai, 201306, China*

†Corresponding Author Email: jiahw@dhu.edu.cn

ABSTRACT

The present study investigated the transmission of exhaled particles generated by coughing inside a car cabin, considering eleven different window opening configurations. The results indicated that particle dispersion and removal were mainly affected by the airflow, which was largely determined by the window opening configurations. Notably, efficient ventilation and a large number of open windows did not necessarily result in lower infection risk. Given the complex structure and formation of intricate airflow patterns within the cabin, airborne particles could spread throughout the cabin and deposit on the interior walls. As particles tended to escape or deposit rapidly within the first 10 s, precautionary measures were necessary during this time frame following a passenger's coughing activity. Furthermore, closing the window adjacent to the driver effectively reduced the proportion of exhaled particles passing through the driver's breathing zone due to the rear-in and front-out airflow pattern, thus mitigating the risk of infection.

Article History

Received November 2, 2023
Revised February 22, 2024
Accepted March 11, 2024
Available online May 29, 2024

Keywords:

Exhaled particle
Window opening
Ventilation
Respiratory disease
Computational fluid dynamics

1. INTRODUCTION

Respiratory infectious diseases are characterized by widespread and high contagiousness and are extremely common in clinical practice (Zhang, 2020). Serious infectious diseases such as varicella, measles, influenza, and tuberculosis are spread primarily by aerosol transmission (Han et al., 2023). Airborne transmission has also been shown to be the primary mode of transmission of COVID-19, which had the widest and most rapid global spread in recent years (Zhang et al., 2020; Li et al., 2021). Therefore, understanding the airborne transmission behaviour of viruses and investigating possible approaches for disrupting airborne pathways is currently the focus of research in biomedicine, built environments, and applied fluids.

Virus aerosols are mainly composed of virus-carrying droplets produced by human expiratory behaviour (e.g. breathing, talking, coughing, sneezing) and their sizes are mainly in the range of 1 to 100 μm. Large-size droplets evaporate quickly to form small-size particles, while those smaller than 5 μm can remain suspended in the air for long periods of time (van Doremalen et al., 2020). Some scholars have suggested that ensuring a social distance of 6 ft and high ventilation efficiency alone cannot reduce the risk of viral transmission (Rencken et al., 2021). Although ventilation can remove virus-carrying particles by controlling airflow, improper ventilation can also spread particles around susceptible individuals (Shao et al., 2021). Therefore, many studies have focused on optimising ventilation settings. Ren et al. (2021) investigated the effects of three different ventilation methods on aerosol dispersion in isolation wards and analysed the behaviour of particles of different sizes. They found that adequate outlet disposition allowed for the effective elimination of larger particles. Li et al. (2011) evaluated the inhalation doses of infectious droplets in susceptible individuals using different ventilation methods. The lowest inhalation dose was obtained for small particles under displacement ventilation; however, for larger particles, the lowest inhalation dose was obtained with an under-floor air distribution system. Kong et al. (2021) compared exposure to infectious particles with different air distribution and ward patterns and proposed an optimal ventilation strategy. In addition, for common ventilation modes (mixed ventilation and displacement ventilation), scholars have analysed the effects on the transmission of exhaled contaminants in different application scenarios, such as airplane cabins (You et al., 2018; Cao et al., 2022), elevator cabins (Li & Feng, 2023), offices (Hatif et al., 2023), and isolation wards (Qian et al., 2006; Qian & Li, 2010).

NOMENCLATURE

ACH	Air Change per Hour	p	pressure
CFD	Computational Fluid Dynamics	k	turbulence kinetic energy
COVID-19	Coronavirus disease 2019	ε	turbulent dissipation ratio
DPM	Discrete Phase Model	t	time
SARS-CoV-2	Severe Acute Respiratory Syndrome coronavirus 2	u_i, u_j	velocity components
FR	front right zone of cabin	x_i, x_j	Cartesian direction
FL	front left zone of cabin	ρ	fluid density
RR	rear right zone of cabin	ρ_p	particle density
RL	rear left zone of cabin	d_p	particle diameter
wlf	left front window	m_p	particle mass
wlr	left rear window	$\boldsymbol{u}$	fluid phase velocity
ws	sunroof	$\boldsymbol{u}_p$	particle velocity
wrf	right front window	μ	fluid viscosity
wrr	right rear window	μ_t	turbulent viscosity
a_1, a_2, a_3	constants	μ_{eff}	effective turbulent viscosity
$C_{1\varepsilon}$, $C_{2\varepsilon}$	model constants	τ_r	particle relaxation time
C_d	force coefficient	Σ_w	area domain of the open window
C_μ	turbulent viscosity constant	Ω_c	volume domain of the cabin
G_k	turbulent energy due to the average velocity gradient	dA	area differentiation of Σ_w
L	length of computational domain	dV	volume differentiation of Ω_c
W	width of computational domain	v_n	normal velocity of the open window
H	height of computational domain	α_k	inverse effective Prandtl numbers for k
N_{total}	total number of particles released	α_ε	inverse effective Prandtl numbers for ε
N_{de}	number of particles deposited on the walls of the vehicle and human body	τ	flow time
N_{es}	number of particles discharged through the opening windows	η_0, β	constants
N_{su}	number of particles suspended in the cabin	η_{de}	deposition fraction
$N_{su,b}$	number of particles have suspended in the driver's breathing zone	η_{es}	escape fraction
Re	Reynolds number	η_{su}	suspension fraction
S	scalar measure of deformation tensor	$\zeta_{su,b}$	percentage of suspended particles in the driver's breathing zone
g	gravity		

Taxi and online ride-hailing services have become popular modes of transportation in the post-Covid-19 era. However, traffic congestion and long commuting times may cause drivers and passengers to spend long periods of time together in a vehicle, which is likely to result in a poor in-vehicle environment. Lednicky et al. (2021) isolated SARS-CoV-2 from a car driven by a COVID-19 patient. Their experimental data confirmed the potential risk of SARS-CoV-2 transmission in an enclosed space of a car with closed windows and running air-conditioning, even if the infected individual is minimally symptomatic. Some scholars have investigated the ventilation modes of vehicle air conditioning that can quickly remove contaminants from vehicles. For example, Shinohara et al. (2023) experimentally evaluated the impact of shields and ventilation on the infection risk of bus drivers. It was found that shields decreased aerosol deposition on drivers by 2-3 orders of magnitude, whereas the use of a ventilation fan and air conditioner reduced the driver's exposure to droplet nuclei by 75.3%-91.4%. Chuang et al. (2013) compared three air-conditioning modes: outside air (OA-mode), circulating inside air (IA-mode), and turning off (Off-mode). The findings showed that using OA-mode could improve air quality and reduce in-car particulate matter ($\leq$ 2.5 μm in aerodynamic diameter) levels. Arpino et al. (2022) simulated the spread of aerosols within a vehicle and found that different ventilation methods had distinct effects on aerosol distribution. Specifically, when air was fed through windscreen defroster vents, the particles were more evenly distributed in the cabin, leading to an increased inhalation of particles by the infected individuals. Conversely, when air was fed through the front seat vents, a recirculation zone was created, which hindered particle dispersion. Chang et al. (2018) used the computational fluid dynamics (CFD) method to estimate the minimum outdoor fresh air flow rate required for ensuring indoor air quality in car cabins, proposing a required minimum outdoor fresh air flow rate of 3.6 l/s per occupant under a CO_2 concentration of 1000 ppm in the cabin.

Owing to the structural limitations of cars, there are

limited ways to change the ventilation pattern of onboard air conditioning systems; therefore, people often choose to open windows to improve ventilation and reduce the risk of infection. Opening windows is an effective and low-cost method to improve ventilation. Mathai et al. (2021, 2022) investigated the transmission of disease-causing contaminants between occupants under various window opening configurations. They found that the flow rate in the vehicle was mainly driven by the external surface pressure distribution of the vehicle and that the relative concentration of vehicle aerosols was inversely proportional to the vehicle speed. Sen and Singh (2021) considered the effects of particle size, window opening configuration, vehicle speed, and lateral ambient wind on particle transmission. They reported that aerosols could leave through one window and then return through another when all windows were open. Shu et al. (2022) investigated the optimal solution that involved opening and closing the windows of a vehicle at different speeds to improve the ventilation efficiency. The results showed that this was not always the best choice when all windows were fully opened. They also assessed the effectiveness of other preventive measures including masks, taxi interior baffles, and air-conditioning systems. It was concluded that face masks were effective, whereas taxi screens and air conditioner systems performed poorly. The previous computational studies oversimplified particles by treating them as tracer gases. These studies also neglected various factors such as seats, mirrors, and human bodies, which might result in significant deviations between the predicted flow field and the actual situation. Therefore, it is essential to investigate the dispersion and distribution of particles using more accurate cabin models and assess the impact of open windows on the risk of infection in vehicles.

In this study, we used numerical calculations to investigate the dispersion characteristics of exhaled particles in a vehicle, considering a range of window opening configurations. The aim of this research was to define the removal efficiency of exhaled particles for different window opening configurations, thereby providing a reference for vehicles on the road to use windows effectively.

2. NUMERICAL METHOD

The Eulerian–Lagrangian method was used to simulate aerosol dispersion. The Eulerian method was used to calculate the airflow, and the Lagrangian method was used to capture the trajectories and motions of discrete exhaled particles (Zhang & Li, 2012; Hassan & Megahed, 2021; Peng et al., 2021; Liu et al., 2022; Zhao et al., 2022). Simulations were performed using the commercial software ANSYS Fluent 2019R1.

The RNG k-ε turbulence model was selected for this study as it had been demonstrated to accurately simulate turbulent airflow both inside (Mao et al., 2018; Bandi et al., 2021), and outside (Cai et al., 2020; Wang et al., 2023a) the vehicle.

The transmission equations corresponding to the turbulent kinetic energy k and dissipation rate ε are:

$$\frac{\partial}{\partial t}(\rho k)+\frac{\partial}{\partial x_i}(\rho k u_i)=\frac{\partial}{\partial x_j}\left(\alpha_k \mu_{eff}\frac{\partial k}{\partial x_j}\right)+G_k-\rho\varepsilon \tag{1}$$

$$\begin{aligned}&\frac{\partial}{\partial t}(\rho\varepsilon)+\frac{\partial}{\partial x_i}(\rho\varepsilon u_i)=\frac{\partial}{\partial x_j}\left(\alpha_\varepsilon \mu_{eff}\frac{\partial \varepsilon}{\partial x_j}\right)\\&+C_{1\varepsilon}\frac{\varepsilon}{k}G_k-\left(C_{2\varepsilon}+\frac{C_\mu\eta^3(1-\eta/\eta_0)}{1+\beta\eta^3}\right)\rho\frac{\varepsilon^2}{k}\end{aligned} \tag{2}$$

where G_k is the turbulent kinetic energy generation rate induced by the mean velocity gradient and can be expressed as

$$G_k=\mu_t S^2 \tag{3}$$

The turbulent viscosity constant C_μ has a value of 0.0845. The other model constants, $C_{1\varepsilon}$ and $C_{2\varepsilon}$, are 1.42 and 1.68, respectively. α_k and α_ε are the inverse effective Prandtl numbers for k and ε, respectively. μ_{eff} is the effective turbulent viscosity. $\eta = Sk/\varepsilon$. S is a scalar measure of the deformation tensor. The constants η_0 and β are 4.38 and 0.012, respectively. μ_t is the turbulent viscosity, which is expressed as

$$\mu_t=\rho C_\mu\frac{k^2}{\varepsilon} \tag{4}$$

The discrete phase model (DPM) was used to solve the motion of exhaled particles, and its governing equation is

$$\frac{d\boldsymbol{u}_p}{dt}=\frac{\boldsymbol{u}-\boldsymbol{u}_p}{\tau_r}+\frac{\boldsymbol{g}\left(\rho_p-\rho\right)}{\rho_p} \tag{5}$$

where $\boldsymbol{u}$ is the fluid phase velocity; $\boldsymbol{u}_p$ is the particle velocity; ρ denotes the fluid density; ρ_p is the particle density; and the first term on the right-hand side of the equation is the resistance term, where τ_r is the droplet relaxation time, which can be written as

$$\tau_r=\frac{\rho_p d_p^2}{18\mu}\frac{24}{C_d\,\mathrm{Re}} \tag{6}$$

where μ is the dynamic viscosity of the fluid; d_p denotes the particle diameter; and Re is the Reynolds number, which is defined as

$$\mathrm{Re}\equiv\frac{\rho d_p\left|\boldsymbol{u}_p-\boldsymbol{u}\right|}{\mu} \tag{7}$$

C_d is the drag coefficient and its expression is

$$C_d=a_1+\frac{a_2}{\mathrm{Re}}+\frac{a_3}{\mathrm{Re}^2} \tag{8}$$

where a_1, a_2, and a_3 are determined by the values derived from the Morsi-Alexander model (Morsi & Alexander, 1972; ANSYS, 2018).

3. COMPUTATIONAL MODEL AND BOUNDARY CONDITIONS

3.1 Geometric Model and Boundary Conditions

The vehicle studied in this work was a left-hand-drive

sedan measuring 4800 mm × 1700 mm × 1450 mm (L × W × H), as shown in Fig. 1(a). The human body, seats, five windows (including four side windows and a sunroof), and rearview mirrors were modeled to match physical reality. Our case study focused on a passenger seated on the right side of the back row. This scenario was considered the greatest possible social distance between drivers and passengers, representing a common scenario in the post-COVID-19 era where the concept of social distancing was widely accepted. It was also assumed that passengers were infected.

The dimensions of the external flow field computational region were based on the study by Zhang et al. (2017) to minimise computation while maintaining the accuracy of the external flow field. The dimensions were set as 10 L × 5 W × 5 H, and the vehicle was positioned at the inlet of the computational domain at a distance of 3 L, as shown in Fig. 1(b).

According to Special Expert Group for Control of the Epidemic of Novel Coronavirus Pneumonia of the Chinese Preventive Medicine Association (Li et al. 2020), respiratory viruses are transmitted mainly through droplets generated by respiratory activities. In particular, 78% of the individuals infected with SARS-CoV-2

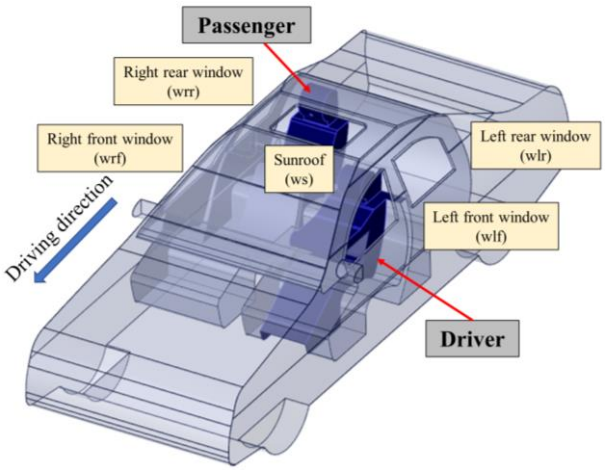

(a)

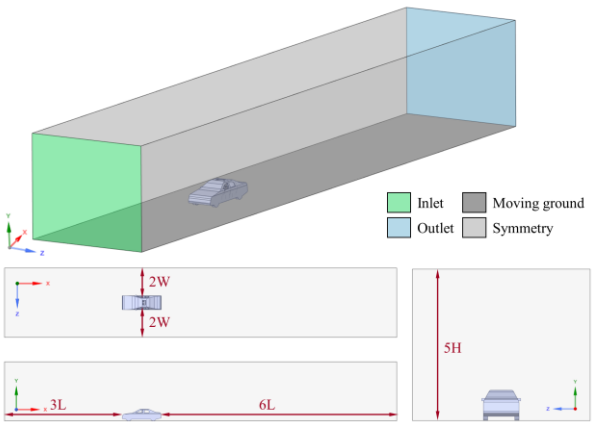

(b)

Fig. 1 Schematic diagram used in this study: (a) car model; (b) external flow field calculation domain

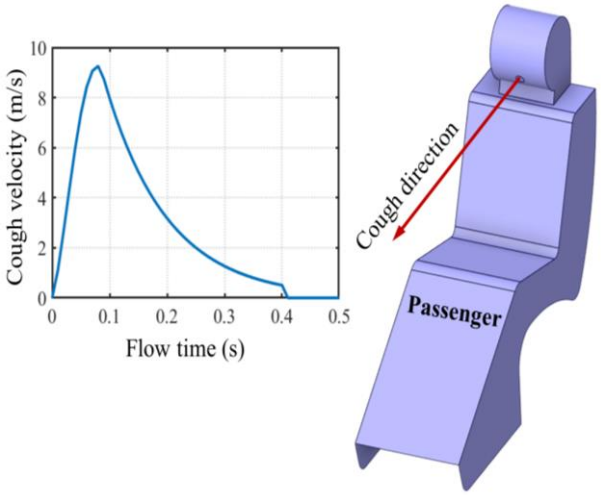

Fig. 2 Passenger-generated cough velocity profile (Gupta et al., 2011) with cough directed straight ahead

experience coughing symptoms and generate large quantities of droplets. Droplet nuclei, formed by droplet evaporation, usually have a particle size of less than 1 μm and contribute significantly to airborne transmission of respiratory diseases (Dai & Zhao, 2021). Therefore, when the concentration of exhaled particles in a car is high, opening the windows is a convenient way to ventilate the car and rapidly decrease the concentration of exhaled particles in the cabin.

In the present study, 1 μm spherical exhaled particles were chosen to model, which had been used previously for aerosol transmission analyses in indoor (Cao et al., 2022; Luan et al., 2022) and cabin environments (Wu et al., 2023). The total number of exhaled particles released from a single cough was set at 5000, following Zhang's (2021) recommendations. For simplification, the mouth of the passenger was considered a circle with a diameter of 0.3 m. Exhaled particles were ejected from the mouth during coughing. Based on previous studies (Yan et al., 2019; Liu et al., 2022; Wang et al., 2023b) the time step was set to 0.01 s. In addition, the airflow velocity at the mouth varied over time based on the empirical curve proposed by Gupta et al. (2011), as shown in Fig. 2, which indicated that the cough lasted for 0.4 s. The boundary conditions for the car body, human body, and computational domain are listed in Table 1.

3.2 Simulation Case

Eleven typical window opening configurations were studied in the present study, as shown in Table 2 (abbreviations of windows correspond to Fig. 1(a)). The driving speed of the vehicle was set to 80 km/h (approximately 22.22 m/s). Cases 1 and 2 involve the opening of a single window, whereas Cases 3 and 4 involve the opening of diagonally opposite windows. In Cases 5 and 6, the sunroof was opened in addition to a single-side window, whereas Case 7 involved the opening of the same side. Cases 8 and 9 involved opening diagonally opposite windows along with the sunroof. Case 10 opened four side windows, and Case 11 opened all five windows.

Table 1 Summary of boundary condition parameters

	Boundary condition	
Interior domain	Bodies of car and humans	No-slip wall
	Closed window	No-slip wall
	Opening window	Interface
	Mouth	Velocity-inlet with cough speed, cough direction was straight ahead
Exterior domain	Inlet	Velocity-inlet with the driving speed 80 km/h
	Outlet	Pressure-outlet with 0 Pa
	Ground	Moving ground with the driving speed 80 km/h
	Other boundaries	Symmetry

Table 2 Summary of window opening configurations

Case No.	The opening windows				
1	ws	/	/	/	/
2	wrr	/	/	/	/
3	wlf	wrr	/	/	/
4	wrf	wlr	/	/	/
5	wlf	ws	/	/	/
6	ws	wrr	/	/	/
7	wrf	wrr	/	/	/
8	wlf	ws	wrr	/	/
9	wrf	ws	wlr	/	/
10	wrf	wlf	wrr	wlr	/
11	wrf	wlf	wrr	wlr	ws

3.3 Assessment Index

To quantify the migration and dispersion of the exhaled particles, the deposition, escape, and suspension fractions were defined as follows:

$$\eta_{de} = N_{de} / N_{total} \tag{9}$$

$$\eta_{es} = N_{es} / N_{total} \tag{10}$$

$$\eta_{su} = N_{su} / N_{total} \tag{11}$$

where N_{total} is the total number of released exhaled particles. N_{de}, N_{es}, and N_{su} denote the numbers of particles deposited on the walls, discharged through the windows, and suspended in the cabin, respectively. To perform visual comparison of the driver's infection risk, the driver's respiratory zone was defined as a spherical volume domain centred at the nose with a radius of 0.2 m (Liu et al., 2022). The risk of infection for the driver could be assessed by calculating the proportion of suspended particles in the driver's breathing zone:

$$\zeta_{su,b} = N_{su,b} / N_{total} \tag{12}$$

where $N_{su,b}$ is the number of particles that have been suspended in the driver's breathing zone during the τ moment.

In addition, the air change per hour (ACH) was utilised as an evaluation index to assess the effectiveness of the vehicle interior ventilation (Teppner et al., 2014). The expression for ACH used in this study is as follows:

$$\mathrm{ACH} = \int_{\Sigma_w} 3600 v_n dA \Big/ \int_{\Omega_c} dV \tag{13}$$

where v_n represents the normal velocity of the open window and is a component of the local velocity vector normal to the window. Σ_w denotes the domain of the open window, and Ω_c is the domain of the cabin. In addition, dA is the area differentiation of Σ_w, and dV is the volume differentiation of Ω_c.

3.4 Grid Sensitivity

An unstructured tetrahedral mesh was used in this study. The mesh was locally refined in the human body as well as in the interior and exterior walls of the vehicle, as shown in Fig. 3(a). To evaluate the mesh sensitivity, the results for Case 3 at a speed of 80 km/h were compared for four different mesh densities with total element count of 0.49 million, 0.97 million, 2.14 million, and 3.26 million. The velocity profiles for the four mesh densities on the schematic sample line running through the center of the front windows (elevation of 1.1 m from the ground) are presented in Fig. 3(b). The calculated results for the four grids were comparable, with 2.14 million grids being the most accurate match to the 3.26 million results. In addition, Fig. 3(c) compared the particle states of the four mesh densities at 20 s in Case 3. The four mesh densities exhibited similar particle-state distributions. In this study, approximately 2.14 million grids were chosen to reduce the computation time without compromising computational accuracy.

4. Results and Analysis

4.1 Exhaled Particle Suspension Distribution

As exhaled particles suspended in air were likely to be inhaled directly by humans, they were the main focus of airborne research (Wang et al. 2021). Fig. 4 shows the variation in the distribution of suspended exhaled particles in the cabin over time for several typical cases with open windows. There was evident that particle movement was significantly influenced by the airflow generated by different window opening configurations. At 0.1 s, exhaled particles began to be released from the mouth into the cabin, and then began to migrate under the influence of the airflow. After 2 s, the particles spread gradually throughout the cabin. Simultaneously, some of the particles were transported away from the cabin by airflow through the open windows and into the external environment.

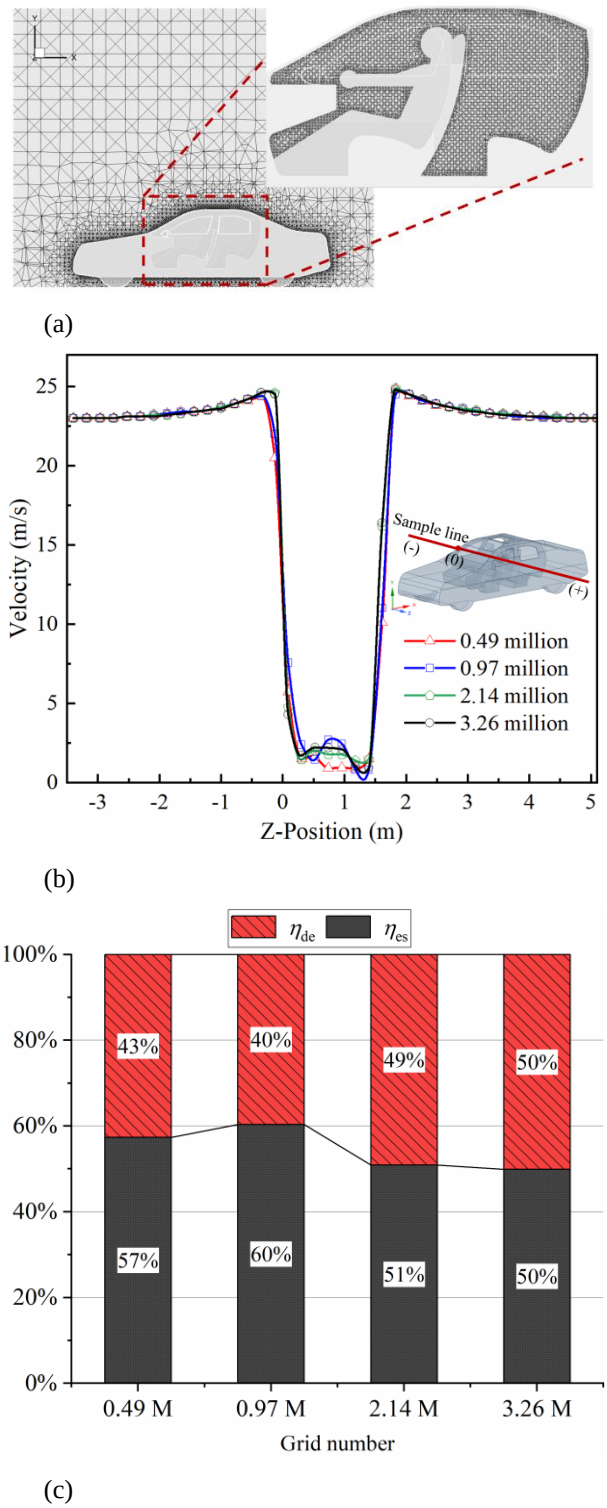

Fig. 3 Grid sensitivity analysis: (a) grid of the inner and outer basin of the car; (b) comparison of speeds on the sampling line shown; (c) particle state at 20 s

In Case 2, where only one passenger window was open, particles were predominantly suspended in the rear area. This was mainly because the open right rear window acted as both an air inlet and outlet, resulting in a concentrated airflow pattern around this window. Consequently, the front area experienced less airflow impact, causing the majority of exhaled particles to remain confined within the rear area.

In Case 3, in which two diagonally opposite windows were opened, the streamlines clearly show the airflow entering through the rear window and exiting through the front window. Figure 5 shows the pressure and normal velocity distributions of the open windows in Case 3. The coupling effect between the internal and external domains generated specific pressure and velocity distributions. Air flowed from the high-pressure region of the open right rear window (wrr) to the low-pressure region of left front window (wlf). Mathai (2021) also reported this phenomenon. As the particle release point was close to the rear window that served as the airflow inlet, the particles were dispersed rapidly within 0.1 s. By contrast, the diversion effect of the front window further promoted the migration of exhaled particles, with some particles escaping through the front window at 2 s. Thus, the position of the release point in the airflow trajectory affected the exclusion of exhaled particles.

In Case 8, which was similar to Case 3 but also included an open sunroof, the rear window functioned as an inlet, whereas both the front window and sunroof served as outlets. Consequently, the sunroof accelerated the particle removal. At 2 s, the concentrations of particles in the car were lower than those in Case 3.

In contrast, Cases 10 and 11, which featured the most number of open windows, were unable to effectively eliminate contamination owing to the chaotic airflow in the cabin. It could be observed that at 1 s, the particle distribution in the cabin was similar to that in Case 8. Therefore, increasing the number of open windows did not necessarily expedite the removal of particles from the cabins.

The streamlines and particle suspension distributions for the other six cases were presented in the *Supplementary File*. In general, the particles tended to be distributed throughout the cabin owing to the airflow dynamics. An efficient discharge could reduce the number of suspended particles, thereby minimising the risk of infection. Hence, it was feasible to minimise the particle suspension levels in a timely manner by strategically selecting window opening configurations and establishing an optimal airflow trajectory.

4.2 Exhaled Particle Deposition Distribution

Because viruses associated with infectious respiratory diseases, such as SARS-CoV-2, could survive in aerosols for up to 3 h and on the surface for several days (van Doremalen et al., 2020), there was a high potential for secondary transmission of viruses when these deposited aerosols were resuspended (Assaad et al. 2020). Therefore, particle deposition was quantified in this study.

Figure 6 shows the distribution of particles deposited in different window opening configurations under typical conditions when the particle state no longer changes. The blue dots represent the deposition locations of the particles on the interior walls of the cabin. As shown in Fig. 6, the deposition of exhaled particles in different window opening configurations was concentrated in distinct areas. For instance, in Case 2, most of the exhaled particles were deposited on the bodies of passengers because of being mainly concentrated in the rear area. The distributions for

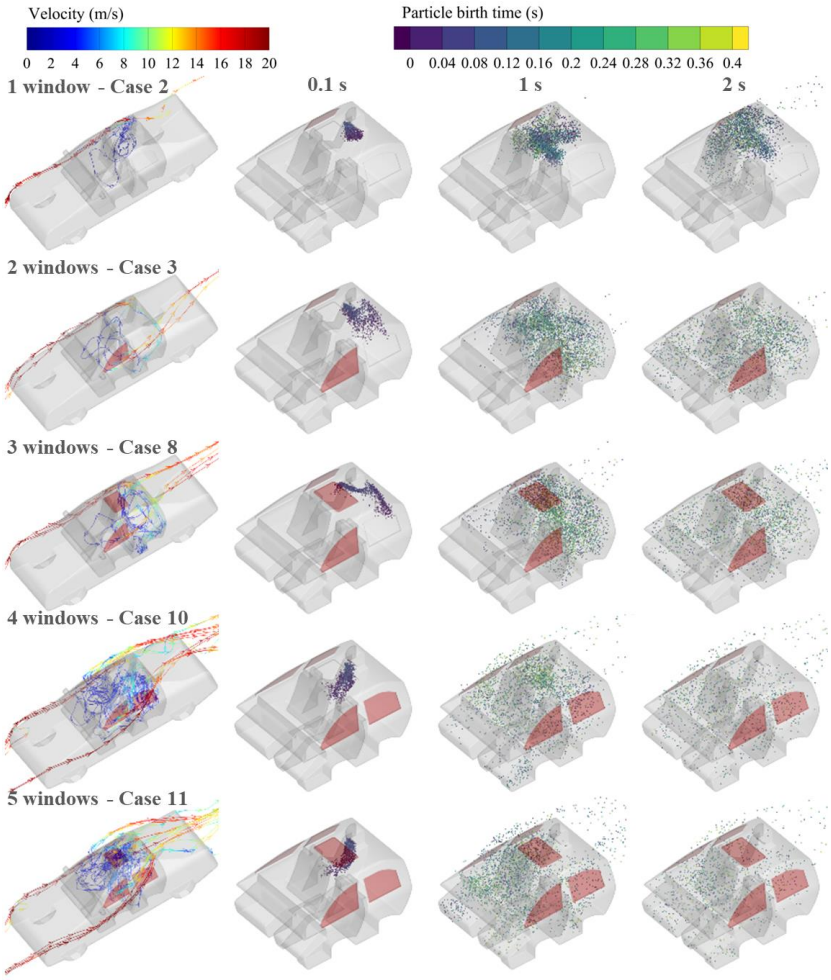

Fig. 4 Streamlines and particle suspension distributions for different window opening configurations

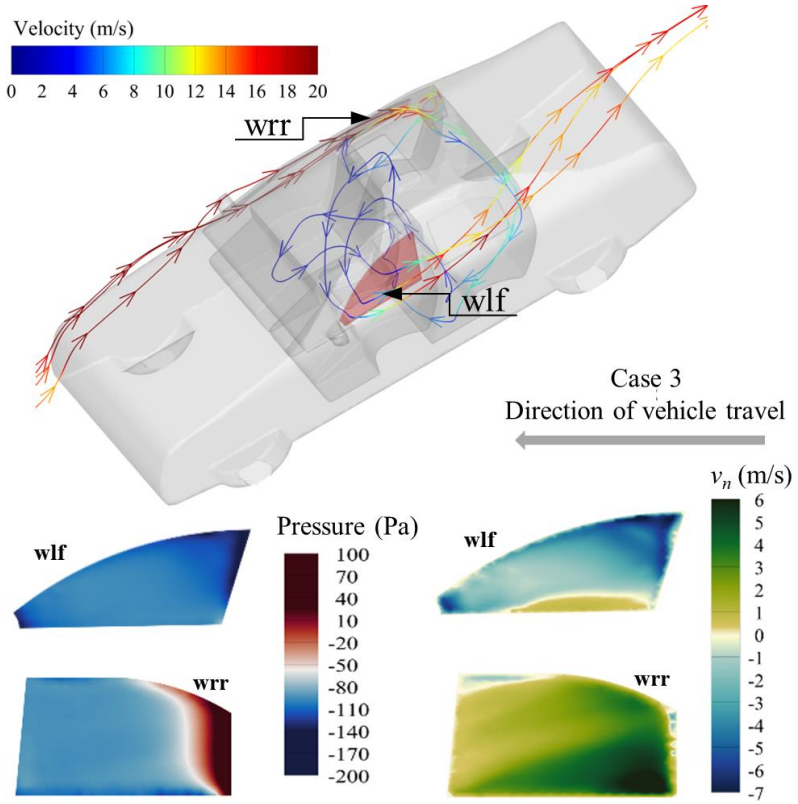

Fig. 5 Streamlines and contours of pressure and normal velocity at the window openings for Case 3

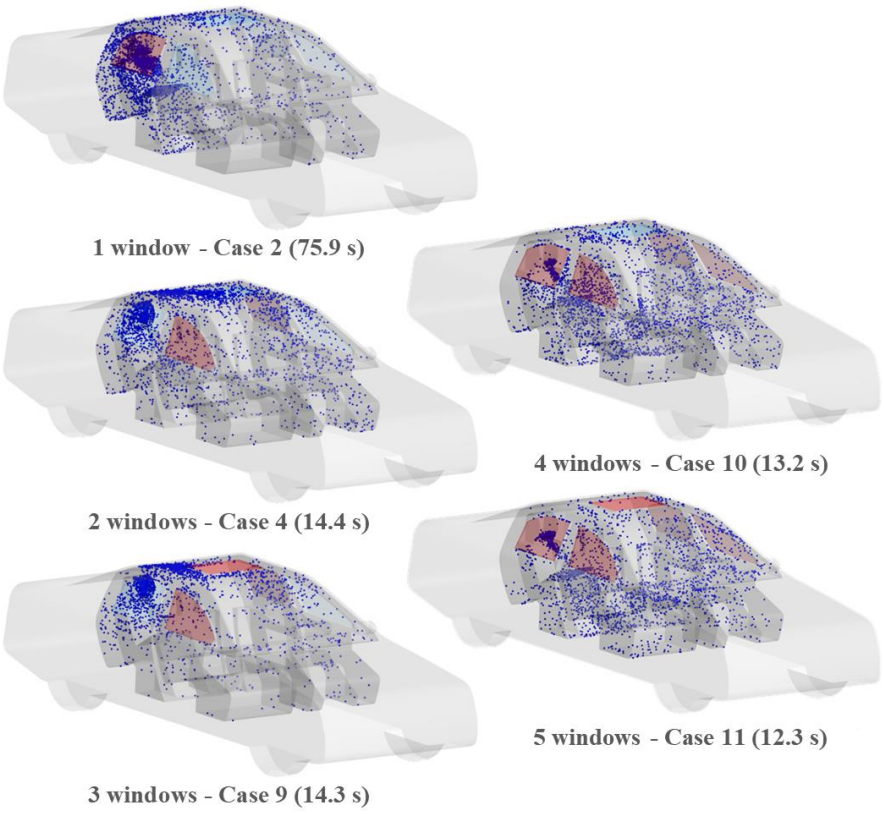

Fig. 6 Deposition distributions of particles for different window opening configurations when the particle state no longer changes (the end times are marked in parentheses)

Cases 4 and 9 were characterised by predominant deposition on the cabin ceiling. This was because the airflow entering through the left rear window blew toward the passengers, carrying the released particles, and subsequently blew some of them toward the cabin ceiling as it moved around the front seats. In contrast, the deposition of particles in Cases 10 and 11 was considerably more extensive, spreading across the interior walls of the cabin. The deposition distributions for the remaining cases could also be found in the *Supplementary File*.

Figure 7 summarises the fractions of exhaled particles deposited on the bodies of the driver and passengers. It could be observed that the proportion of particles deposited on the bodies of passengers was much larger than that on the driver's body. The deposition fractions on the driver's body were below 4%, with Case 6 (with the sunroof and driver side window open) achieving the lowest deposition fraction of 0.8%. However, the deposition fraction on the passenger's body was relatively large in Case 6, and reached nearly 40 times that of the deposition fraction on the driver's body in Case 2. In contrast, the deposition fraction on the driver's body was greater than 3% in Case 5, in which the sunroof and passenger-side window were open, and in Cases 10 and 11, in which all windows were open. Hence, increasing the number of open windows did not necessarily reduce the risk of infection.

To analyse the deposition characteristics of the exhaled particles, we divided the cabin into four zones: passenger (RR), front right (FR), rear left (RL), and driver

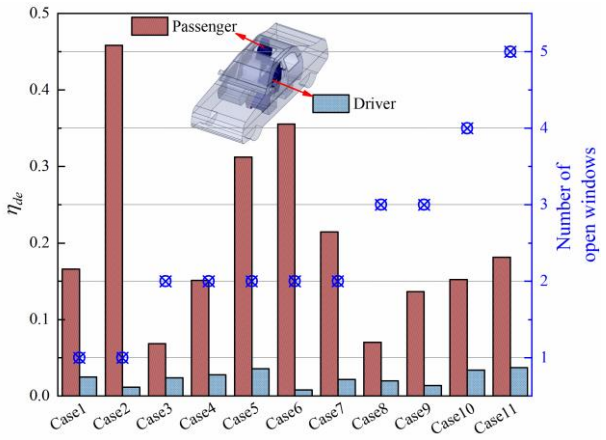

Fig. 7 Particle deposition fractions on human bodies

(FL). The deposition fractions in each zone were calculated, as shown in Fig. 8. Additionally, the amount of deposition on the human body was excluded from the analysis. It could be seen that the deposition of exhaled particles was highest in the RR zone, with an average value of approximately 0.186. In some cases, owing to the impact of the airflow path, the deposition fractions in the RL area exceeded 0.2, for example, in Cases 1, 3, and 8. However, in Cases 4 and 9, the RL region exhibited the smallest deposition fraction among the four areas. Therefore, the deposition fraction in the RL area varied considerably depending on the window opening configuration. In addition, the total deposition fractions in the front regions (FR and FL) were lower than those in the

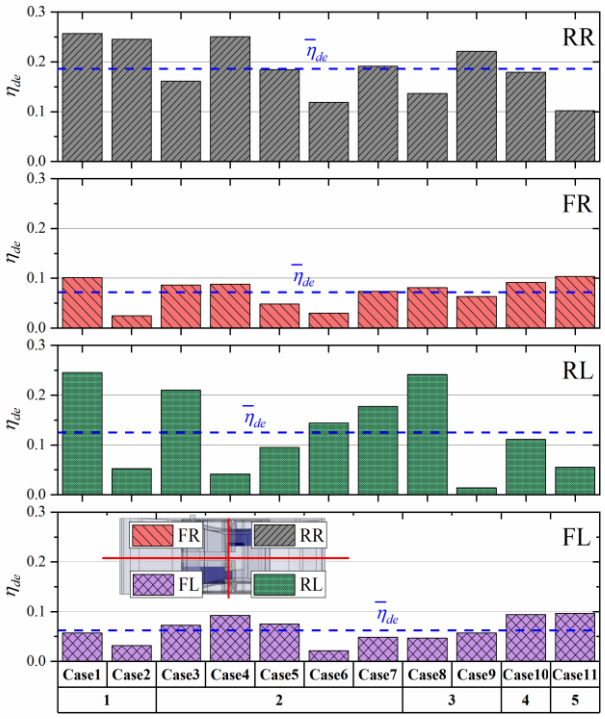

Fig. 8 Particle deposition fractions for four areas in the cabin (without particle depositions on the human body)

rear areas (RR and RL), with most FR and FL deposition fractions being below 0.1. Therefore, when performing operations such as sterilization, priority should be given to the rear areas (RR and RL) because it was important to avoid indirect transmission or resuspension of virus-containing particles after exposure (Dhand & Li, 2020). Furthermore, there was no obvious correlation between the number of open windows and the deposition fraction; therefore, specific cases need to be analysed on a case-by-case basis.

In summary, deposition distribution was related to suspension distribution. The complex internal structure of the cabin led to a convoluted airflow pattern, resulting in potential particle deposition on across the interior walls of the cabin. However, a higher fraction of particle deposition was observed in the rear area of the vehicle, which should be prioritised for sterilisation.

4.3 Quantitative Analysis of Exhaled Particle Removal Effect

To compare the particle status of individual cases more intuitively and further analyse the infection risk, this study counted the assessment indices at different moments, as shown in Fig. 9. Taking Case 1 as an example, Fig. 9(a) illustrated the correlation between the four assessment indices. η_{de}, η_{es}, and η_{su} were summed to 100%. It could be seen that at 59.3 s all the particles in the vehicle had either deposited or escaped. In addition, the blue line represented the total number of particles that were suspended in the breathing zone $\zeta_{su,b}$. The line continued to rise cumulatively and stopped rising at 25 s. A comparison of $\zeta_{su,b}$, η_{es}, and η_{de} for each case was shown in Fig. 9(b), (c), and (d), respectively.

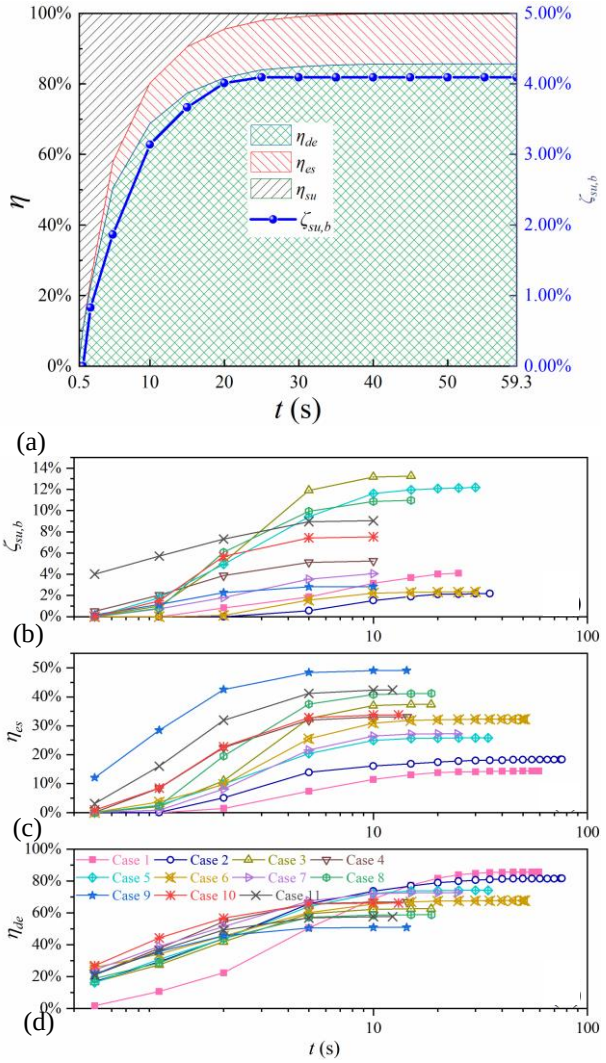

Fig. 9 Particle states in different cases

As shown in Fig. 9(b), $\zeta_{su,b}$ increased gradually and eventually stabilised when the concentration of pollutants in the driver's breathing zone ceased to increase. Cases 3, 5, 8, 10, and 11 corresponded to scenarios in which the window next to the driver was open (wlf). In these cases, more than 7% of the exhaled particles reached the driver's breathing zone, resulting in a higher risk of infection. In the remaining six cases, $\zeta_{su,b}$ was < 5%. Notably, in Case 2, $\zeta_{su,b}$ was less than 2%. This was because the primary airflow path in the vehicle did not pass through the driver's breathing zone, and the low airflow inside the vehicle limited the diffusion of contamination.

Higher escape fractions (η_{es}) and lower deposition fractions (η_{de}) were both beneficial for minimising the risk of infection within a vehicle. As shown in Fig. 9(c) and (d), Cases 10 and 11, which had four and five open windows, respectively, exhibited the earliest cessation of the particle state transitions. Additionally, Case 9 showed the highest value of η_{es} at 50%, yet it also achieved stabilisation early. This implied that if wrf, wlr, and ws were opened simultaneously, the infection probability could be significantly reduced within approximately 14 s. Moreover, from η_{de}, it was evident that particles tend to

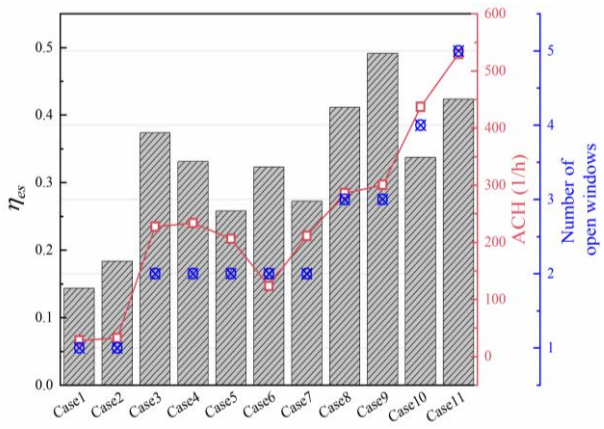

Fig. 10 Comparison of particle escape fraction η_{es} with ACH

deposit rapidly within the initial 10 s in most scenarios. Consequently, precautions should be primarily focused on the first 10 s following the onset of passenger coughing.

The relationship between η_{es} and ACH, as depicted in Fig. 10, exhibited a discernible correlation. Specifically, an increase in ACH tended to promote an increase in η_{es}. However, some instances had deviated from this trend. For instance, Case 6 displays a lower ACH value compared to Cases 5 and 7, yet its η_{es} surpassed that of these two cases. This discrepancy could be attributed to the fact that the particle release point in Case 6 was close to the airflow inlet, which allowed the particles to escape rapidly through the sunroof. Furthermore, while Cases 10 and 11 (with four and five open windows, respectively) achieved the highest ACH values, their internal airflow patterns rendered them inefficient for exhaled-particle discharge. Among the other window opening configurations, the escape fractions of the case with one window open (Cases 1 and 2) were small, followed by the case with two windows open, whereas the escape fractions of the case with three windows open (Cases 8 and 9) and five windows open (Case 11) were the largest. Additionally, when considering Fig. 8 along with this information, it was evident that Cases 1, 2, and 6 had the longest durations of particle state change, and also showed the lowest ACH values. Therefore, poor ventilation efficiency not only reduced escape fraction of exhaled particles but also prolonged suspension of residual particles within the vehicle.

5. CONCLUSION

This study analysed the diffusion behaviour of exhaled particles released by passenger coughing under different window opening configurations using numerical simulations. The following conclusions were drawn.

(1) Exhaled particles were primarily influenced by the airflow, with various window opening configurations exhibiting distinct airflow patterns. The relationship between the number of open windows and particle escape fraction was not straightforward. Therefore, selecting an appropriate window opening configuration could accelerate the reduction in the number of suspended particles.

(2) Owing to the complex structure of the cabin interior and complex airflow, the particles spread throughout the cabin with the airflow. Therefore, the entire surface area of the interior walls of the cabin could serve as an area for particle deposition. Hence, there was a need for proper disinfection of cabin interiors.

(3) According to the simulation results, the particles either escaped rapidly or deposited within the first 10 s in most cases. Therefore, precautions must be taken within the first 10 s of the onset of a passenger's coughing activity.

(4) The escape fraction η_{es} of particles was related to the ventilation efficiency. The lower the ventilation efficiency, the smaller the escape fraction, and the longer the residual particles remained suspended in the cabin. However, a higher ventilation efficiency does not necessarily result in a larger η_{es}.

(5) Closing the window next to the driver could effectively reduce the proportion of particles passing through the driver's breathing zone and minimised the probability of infection due to rear-in and front-out airflow patterns.

ACKNOWLEDGEMENTS

This work was supported by the National Natural Science Foundation of China [Grant No. 52006030], Shanghai Sailing Program [Grant No. 18YF1400700], and China Postdoctoral Science Foundation [Grant No. 2018M641891].

CONFLICT OF INTEREST

The authors declare that they have no known competing financial interests or personal relationships that may have influenced the work reported in this study.

AUTHORS CONTRIBUTION

All the authors whose names appear in the submission made substantial contributions to the conception or design of the work and approved the version for publication.

REFERENCES

ANSYS (2018). *Fluent User's Guide*. ANSYS Inc.

Arpino, F., Cortellessa, G., Grossi, G., & Nagano, H. (2021). A Eulerian-Lagrangian approach for the non-isothermal and transient CFD analysis of the aerosol airborne dispersion in a car cabin. *Building and Environment*, *209*, 108648. https://doi.org/10.1016/j.buildenv.2021.108648

Assaad, D. A., Ghali, K. F., Ghaddar, N., & Habchi, C. (2020). Coupled CFD and particle resuspension models under combined effect of mechanical and aerodynamic disturbances. *Building and Environment*, *169*, 106567. https://doi.org/10.1016/j.buildenv.2019.106567

Bandi, P., Paul Manelil, N., Maiya, M., Tiwari, S., Thangamani, A., & Tamalapakula, J. L. (2021). Influence of flow and thermal characteristics on thermal comfort inside an automobile cabin under the effect of solar radiation. *Applied Thermal Engineering*, *203*, 117946. https://doi.org/10.1016/j.applthermaleng.2021.117946

Cai, C., Ming, T., Fang, W., Richter, R.K., & Peng, C. (2020). The effect of turbulence induced by different kinds of moving vehicles in street canyons. *Sustainable Cities and Society*, *54*, 102015. https://doi.org/10.1016/j.scs.2020.102015

Cao, Q., Liu, M., Li, X., Lin, C. H., Wei, D., Ji, S., Zhang, T. T., & Chen, Q. (2022). Influencing factors in the simulation of airflow and particle transportation in aircraft cabins by CFD. *Building and Environment*. *207*, 108413. https://doi.org/10.1016/j.buildenv.2021.108413

Chang, T., Sheu, J., Huang, J., Lin, Y., & Chang, C. (2018). Development of a CFD model for simulating vehicle cabin indoor air quality. *Transportation Research Part D: Transport and Environment*, *62*, 433–440. https://doi.org/10.1016/j.trd.2018.03.018

Chuang, H., Lin, L., Hsu, Y., Ma, C., & Chuang, K. (2013). In-car particles and cardiovascular health: an air conditioning-based intervention study. *Science of The Total Environment*, *452–453*, 309–313. https://doi.org/10.1016/j.scitotenv.2013.02.097

Dai, H., & Zhao, B. (2021). Movement and transmission of human exhaled droplets/droplet nuclei. *Chinese Science Bulletin*, *66*(Z1), 493–500. https://doi.org/10.1360/TB-2020-0643

Dhand, R., & Li, J. (2020). Coughs and sneezes: Their role in transmission of respiratory viral infections, including SARS-CoV-2. *American Journal of Respiratory and Critical Care Medicine*, *202*(5), 635–P18. https://doi.org/10.1164/rccm.202004-1263PP

Gupta, J. K., Lin, C. H., & Chen, Q. (2011). Transport of expiratory droplets in an aircraft cabin. *Indoor Air*, *21*(1), 3–11. https://doi.org/10.1111/j.1600-0668.2010.00676.x

Han, P., Zheng, H., Teng, Y., & Sun, D. (2023). Advances in the study of aerosol transmission of infectious diseases through breathing. *Chinese Journal of Zoonoses*, *39*(02), 153–160. http://www.rsghb.cn/EN/10.3969/j.issn.1002-2694.2022.00.190

Hassan, A. M., & Megahed, N. A. (2021). COVID-19 and urban spaces: A new integrated CFD approach for public health opportunities. *Building and Environment*, *204*, 108131. https://doi.org/10.1016/j.buildenv.2021.108131

Hatif, I. H., Mohamed Kamar, H., Kamsah, N., Wong, K. Y., & Tan, H. (2023). Influence of office furniture on exposure risk to respiratory infection under mixing and displacement air distribution systems. *Building and Environment*, *239*, 110292. https://doi.org/10.1016/j.buildenv.2023.110292

Kong, X., Guo, C., Lin, Z., Duan, S., He, J., Ren, Y., & Ren, J. (2021). Experimental study on the control effect of different ventilation systems on fine particles in a simulated hospital ward. *Sustainable Cities and Society*, *73*, 103102. https://doi.org/10.1016/j.scs.2021.103102

Lednicky, J. A., Lauzardo, M., Alam, M. M., Elbadry, M. A., Stephenson, C. J., Gibson, J. C., & Morris, J. G., Jr (2021). Isolation of SARS-CoV-2 from the air in a car driven by a COVID patient with mild illness. *International Journal of Infectious Diseases*, *108*, 212–216. https://doi.org/10.1016/j.ijid.2021.04.063

Li, L., Liang, X., Jiang, Q., Wang, H., & Wang, B. (2020). Special Expert Group for Control of the Epidemic of Novel Coronavirus Pneumonia of the Chinese Preventive Medicine Association (2020) An update on the epidemiological characteristics of novel coronavirus pneumonia (COVID-19). *Chinese Journal of Epidemiology*, *41*(2), 139–144. https://doi.org/10.3760/cma.j.issn.0254-6450.2020.02.002

Li, X., & Feng, B. (2023). Transmission of droplet aerosols in an elevator cabin: Effect of the ventilation mode. *Building and Environment*, *236*, 110261. https://doi.org/10.1016/j.buildenv.2023.110261

Li, X., Jiang, J., Wang, D., Deng, J., He, K., & Hao, J. (2021). Transmission of coronavirus via aerosols and influence of environmental conditions on its transmission. *Environmental Science*, *42*(07), 3091–3098. https://doi.org/10.13227/j.hjkx.202010033

Li, X., Niu, J., & Gao, N. (2011). Spatial distribution of human respiratory droplet residuals and exposure risk for the co-occupant under different ventilation methods. *HVAC&R Research*, *17*, 432–445. https://doi.org/10.1080/10789669.2011.578699

Liu, S., Zhao, X., Nichols, S. R., Bonilha, M. W., Derwinski, T., Auxier, J. T., & Chen, Q. (2022). Evaluation of airborne particle exposure for riding elevators. *Building and Environment*, *207*, 108543. https://doi.org/10.1016/j.buildenv.2021.108543

Luan, Y., Zhang, L., Yin, Y. Yan, L., Wu, X., & Sun, T. (2022). Ventilation structure optimization and virus spreading law in large indoor places. *Environmental Engineering*, *40*(12), 180–186. https://doi.org/10.13205/j.hjgc.202212024

Mao, Y., Wang, J., & Li, J. (2018). Experimental and numerical study of air flow and temperature variations in an electric vehicle cabin during cooling and heating. *Applied Thermal Engineering*, *137*, 356–367. https://doi.org/10.1016/j.applthermaleng.2018.03.099

Mathai, V., Das, A., & Breuer, K. (2022). Aerosol transmission in passenger car cabins: Effects of ventilation configuration and driving speed. *Physics*

of Fluids, *34*(2), 021904. https://doi.org/10.1063/5.0079555

Mathai, V., Das, A., Bailey, J. A., & Breuer, K. (2021). Airflows inside passenger cars and implications for airborne disease transmission. *Science Advances*, *7*(1), eabe0166. https://doi.org/10.1126/sciadv.abe0166

Morsi, S. A., & Alexander, A. J. (1972). An investigation of particle trajectories in two-phase flow systems. *Journal of Fluid Mechanics*, *55*, 193–208. https://doi.org/10.1017/S0022112072001806

Peng, N. N., Chow, K. W., & Liu, C. H. (2021). Computational study on the transmission of the SARS-CoV-2 virus through aerosol in an elevator cabin: Effect of the ventilation system. *Physics of Fluids*, *33*(10), 103325. https://doi.org/10.1063/5.0068244

Qian, H., & Li, Y. (2010). Removal of exhaled particles by ventilation and deposition in a multibed airborne infection isolation room. *Indoor Air*, *20*(4), 284–297. https://doi.org/10.1111/j.1600-0668.2010.00653.x

Qian, H., Li, Y., Nielsen, P. V., Hyldgaard, C. E., Wong, T. W., & Chwang, A. T. (2006). Dispersion of exhaled droplet nuclei in a two-bed hospital ward with three different ventilation systems. *Indoor Air*, *16*(2), 111–128. https://doi.org/10.1111/j.1600-0668.2005.00407.x

Ren, J., Wang, Y., Liu, Q., & Liu, Y. (2021). Numerical Study of Three Ventilation Strategies in a prefabricated COVID-19 inpatient ward. *Building and Environment*, *188*, 107467. https://doi.org/10.1016/j.buildenv.2020.107467

Rencken, G., Rutherford, E., Ghanta, N., Kongoletos, J., & Glicksman, L. R. (2021). Patterns of SARS-CoV-2 aerosol spread in typical classrooms. *Building and Environment*, *204*, 108167–108167. https://doi.org/10.1016/j.buildenv.2021.108167

Sen, N., & Singh, K. K. (2021). Spread of virus laden aerosols inside a moving sports utility vehicle with open windows: A numerical study. *Physics of Fluids*, *33*, 095117. https://doi.org/10.1063/5.0061753

Shao, S., Zhou, D., He, R., Li, J., Zou, S., Mallery, K., Kumar, S., Yang, S., & Hong, J. (2021). Risk assessment of airborne transmission of COVID-19 by asymptomatic individuals under different practical settings. *Journal of Aerosol Science*. *151*, 105661. https://doi.org/10.1016/j.jaerosci.2020.105661

Shinohara, N., Ogata, M., Kim, H., Kagi, N., Tatsu, K., Inui, F., & Naito, W. (2023). Evaluation of shields and ventilation as a countermeasure to protect bus drivers from infection. *Environmental Research*, *216*(Pt 3), 114603. https://doi.org/10.1016/j.envres.2022.114603

Shu, S., Mitchell, T. E., Wiggins, M. R., You, S., Thomas, H., & Li, C. (2022). How opening windows and other measures decrease virus concentration in a moving car. *Engineering Computations*, *39*(6), 2350–2366. https://doi.org/10.1108/EC-11-2021-0666

Teppner, R., Langensteiner, B., Meile, W., Brenn, G., & Kerschbaumer, S. (2014). Air change rates driven by the flow around and through a building storey with fully open or tilted windows: An experimental and numerical study. *Energy and Buildings*, *76*, 640-653. https://doi.org/10.1016/j.enbuild.2014.07.020

van Doremalen, N., Bushmaker, T., Morris, D. H., Holbrook, M. G., Gamble, A., Williamson, B. N., Tamin, A., Harcourt, J. L., Thornburg, N. J., Gerber, S. I., Lloyd-Smith, J. O., de Wit, E., & Munster, V. J. (2020). Aerosol and surface stability of SARS-CoV-2 as compared with SARS-CoV-1. *The New England Journal of Medicine*, *382*(16), 1564–1567. https://doi.org/10.1056/NEJMc2004973

Wang, C. C., Prather, K. A., Sznitman, J., Jimenez, J. L., Lakdawala, S. S., Tufekci, Z., & Marr, L. C. (2021). Airborne transmission of respiratory viruses. *Science*, *373*(6558), eabd9149. https://doi.org/10.1126/science.abd9149

Wang, D., Sun, M., Shen, X., & Chen, A. (2023a) Aerodynamic characteristics and structural behavior of sound barrier under vehicle-induced flow for five typical vehicles. *Journal of Fluids and Structures*, *117*, 103816. https://doi.org/10.1016/j.jfluidstructs.2022.103816

Wang, T., Shi, F., Shi, F., Li, C., Zhang, L., Wang, J., Jiang, C., Qian, B., Dai, L., & Ji, P. (2023b). Numerical study of the effect of composition models on cough droplet propagation distributions in confined space. *Building and Environment*, *234*, 110117. https://doi.org/10.1016/j.buildenv.2023.110117

Wu, F., Li, X., Cui, Q., Li, H., Fan, Z., & Xu, R. (2023). Investigation on the transmission profile of coughing droplets in passenger compartment of subway train. *Journal of Railway Science and Engineering*, *20* (12), 4529–4540 https://doi.org/10.19713/j.cnki.43-1423/u.T20230162

Yan, Y., Li, X., & Tu, J. (2019). Thermal effect of human body on cough droplets evaporation and dispersion in an enclosed space. *Building and Environment*, *148*, 96–106. https://doi.org/10.1016/j.buildenv.2018.10.039

You, R., Zhang, Y., Zhao, X., Lin, C. H., Wei, D., Liu, J., & Chen, Q. (2018). An innovative personalized displacement ventilation system for airliner cabins. *Building and Environment*, *137*, 41–50. https://doi.org/10.1016/j.buildenv.2018.03.057

Zhang, K. (2020). Main characteristics of respiratory infectious diseases and ways to prevent and control. *Guide of China Medicine*, *18*(01), 102–103. https://doi.org/10.15912/j.cnki.gocm.2020.01.090

Zhang, L., & Li, Y. (2012). Dispersion of coughed droplets in a fully-occupied high-speed rail cabin.

Building and Environment, *47*, 58–66. https://doi.org/10.1016/j.buildenv.2011.03.015

Zhang, R., Li, Y., Zhang, A. L., Wang, Y., & Molina, M. J. (2020). Identifying airborne transmission as the dominant route for the spread of COVID-19. *Proceedings of the National Academy of Sciences of the United States of America*, *117*(26), 14857–14863. https://doi.org/10.1073/pnas.2009637117

Zhang, Y. (2021). *Transmission control mechanism and experimental study of aerosols based on different air distribution in air conditioned rooms*. [PhD. Thesis, Chongqing University], China. https://doi.org/10.27670/d.cnki.gcqdu.2021.003757

Zhang, Z., Li, X., & Cui, X. (2017). Numerical simulation of external flow field of a roadster based on CFD. *Journal of Shandong Industrial Technology*, *12*, 285–287. https://doi.org/10.16640/j.cnki.37-1222/t.2017.12.256

Zhao, X., Liu, S., Yin, Y., Zhang, T. T., & Chen, Q. (2022). Airborne transmission of COVID-19 virus in enclosed spaces: An overview of research methods. *Indoor Air*, *32*(6), e13056. https://doi.org/10.1111/ina.13056